COMMUNICATIONS IN COMPUTATIONAL PHYSICS
Vol. **3**, No. 2, pp. 406-426

Commun. Comput. Phys.
February 2008

Numerical Investigations of the Dynamical Behaviors and Instabilities for the Gierer-Meinhardt System

Zhonghua Qiao*

Center for Research in Scientific Computation, North Carolina State University, Raleigh, North Carolina, 27695-8205, USA.

Received 7 January 2007; Accepted (in revised version) 28 May 2007

Available online 9 October 2007

Abstract. This work is concerned with the numerical simulations on the Gierer-Meinhardt activator-inhibitor models. We consider the case when the inhibitor time constant τ is non-zero. In this case, oscillations and pulse splitting are observed numerically. Numerical experiments are carried out to investigate the dynamical behaviors and instabilities of the spike patterns. The numerical schemes used are based upon an efficient moving mesh finite element method which distributes more grid points near the localized spike regions.

AMS subject classifications: 65M50, 65M60

Key words: Gierer-Meinhardt model, moving finite element method, pulse splitting, spikes.

1 Introduction

The generation of spatial pattern of tissue structures is one of the elementary processes in morphogenesis. Since the pioneering work of Turing [3] in 1952, there have been many studies on two-component reaction-diffusion systems for the formation of spatially complex patterns, see [4, 8, 9, 31]. It has been largely explored that the instabilities of spatially homogeneous patterns can develop varying states via the mechanism of local self-enhancement and long range inhibition. However, in the singularly perturbed limit, many reaction-diffusion systems can give rise to spike-type patterns whereby one of the components of the system becomes spatially localized at certain regions in the domain. In contrast to spatially homogeneous solutions, the instabilities and the dynamics of these localized patterns are not nearly as well understood.

Various models have been proposed for the pattern formation, such as Gray-Scott model [6], Schnakenberg model [7] and Gierer-Meinhardt (GM) model [5]. Among

*Corresponding author. *Email address:* zqiao@ncsu.edu (Z.-H. Qiao)

these models, GM model seems to be the most well-known reaction-diffusion system of activator-inhibitor type. It has been widely used to model localization processes in nature, such as cell differentiation and morphogenesis [1,31], and the formation of sea-shell patterns [2]. The dimensionless GM model can be written as (cf. [10,15])

$$a_t=\epsilon^2\Delta a-[1+V(x)]a+\frac{a^p}{h^q},\quad x\in\Omega,\quad t>0, \tag{1.1}$$

$$\tau h_t=D\Delta h-\mu h+\epsilon^{-N}\frac{a^r}{h^s},\quad x\in\Omega,\quad t>0, \tag{1.2}$$

$$\partial_n a=\partial_n h=0,\quad x\in\partial\Omega, \tag{1.3}$$

$$a(x,y,0)=a^0(x,y),\quad h(x,y,0)=h^0(x,y). \tag{1.4}$$

Here a, h, $0<\epsilon\ll 1$, $D>0$, $\mu>0$, $V=V(x)\geq 0$ and $\tau\geq 0$, represent the scaled activator concentration, inhibitor concentration, activator diffusivity, inhibitor diffusivity, inhibitor decay rate, activator decay rate, and inhibitor time constant, respectively. ∂_n is the outward normal derivative to the boundary, and Ω is a bounded domain in $\mathbb{R}^N$. The exponents (p,q,r,s) are assumed to satisfy

$$p>1,\quad q>0,\quad r>1,\quad s\geq 0,\quad \frac{p-1}{q}<\frac{r}{s+1}. \tag{1.5}$$

For $\epsilon\ll 1$, many studies of GM model have shown the spike patterns become narrower and narrower when $\epsilon\to 0$, see [1,24]. In fact, their spatial extension is of order $\mathcal{O}(\epsilon)$. And the spike patterns also have various dynamical behaviors, such as the drift of the center of the spikes, the oscillation of the height of the spikes, even the splitting of the spikes. So very fine meshes over the spatial extension of the spikes are needed to resolve this problem. Although using a very large number of equidistantly spaced spatial mesh points to solve the spike dynamics is possible in one space dimension, it is computationally inefficient. And for multi space dimensions, it is almost infeasible to simulate multi-spikes dynamics using uniform mesh approach. In viewing of this, some adaptive grid strategies should be applied. In [14], satisfactory numerical solutions for the one-dimensional GM and Schnakenberg model are obtained using the moving mesh method. Moreover, there are also several other works on one-dimensional GM model, see, e.g., [10,11,25,26]. For two-dimensional GM model, some analysis works can be found in [15, 23, 24, 32]. However, because of the extremely large computational cost, there are only a few works in numerical simulations for spike dynamics in 2D, see [10,22,31].

Numerical difficulties in simulating two-dimensional GM model also lie in that there are different orders of errors: the error in spike height is $\mathcal{O}(\frac{1}{\log\frac{1}{\epsilon}})$, the error in spike location is $\mathcal{O}(\epsilon)$, the critical threshold for D is $\mathcal{O}(\log\frac{1}{\epsilon})$ and the time evolution for spikes is $\mathcal{O}(\frac{1}{\epsilon^2\log\frac{1}{\epsilon}})$. The traditional finite element method (FEM) can not resolve the spike dynamics for very small ϵ.

In this paper, we use moving finite element method, introduced in [12,13], to simulate the spike dynamics of the singularity perturbed Gierer-Meinhardt (GM) model in two

space dimension. This paper is organized as follows. In Section 2, we present a moving finite element method to solve a typical case of the GM model numerically. In Section 3, we solve the GM model when $\tau=0$ in two-dimensional domain for the motion of localized spike-type solutions. In Section 4, we solve the GM model when $\tau>0$. Some concluding remarks are given in the final section.

2 Numerical methods

A typical case is $(2,1,2,0)$ for the exponents (p,q,r,s) in (1.5). Then the GM model (1.1)-(1.4) becomes:

$$a_t=\epsilon^2\Delta a-[1+V(x)]a+\frac{a^2}{h},\quad x\in\Omega,\quad t>0, \tag{2.1}$$

$$\tau h_t=D\Delta h-\mu h+\epsilon^{-2}a^2,\quad x\in\Omega,\quad t>0, \tag{2.2}$$

$$\partial_n a=\partial_n h=0,\quad x\in\partial\Omega, \tag{2.3}$$

$$a(x,y,0)=a^0(x,y),\quad h(x,y,0)=h^0(x,y). \tag{2.4}$$

In this work, we will employ finite element methods together with moving mesh strategy to solve problem (2.1)-(2.4). Using the moving mesh strategy, we can move mesh points into the spatial extension of the spikes. Moreover, the mesh can move following the dynamical behaviors of the spikes.

There have been several works using moving mesh methods for solving various physical problems, see, e.g., [16–18]. These moving mesh methods are quite different in their designing strategies, see, e.g., [19–21]. In this work, we will follow the moving mesh strategy proposed in [12,13]. One of the primary features of the approach we adopted is that the mesh redistribution part and the PDE evolution part are separated. It allows us to use any appropriate PDE solver which is irrelevant with the adaptive method.

2.1 PDE solver

In this subsection, we describe the PDE solver used in this paper. For simplicity, we write (2.1)-(2.2) in the compact form

$$M\mathbf{u}_t=K\Delta\mathbf{u}+\mathbf{f}(\mathbf{u},\mathbf{x}), \tag{2.5}$$

where $\mathbf{u}=(a,h)$ and

$$M:=\begin{pmatrix}1&0\\0&\tau\end{pmatrix},\quad K:=\begin{pmatrix}\epsilon^2&0\\0&D\end{pmatrix}, \tag{2.6}$$

$$\mathbf{f}(\mathbf{u},\mathbf{x}):=\begin{pmatrix}-[1+V(x)]a+\frac{a^2}{h}\\-\mu h+\epsilon^{-2}a^2\end{pmatrix}. \tag{2.7}$$

For the space discretization, we use the linear finite element approximation. Let $\Gamma=\{\kappa\}$ be a finite element partition of Ω into triangular element κ. Now we define the linear finite element space

$$S_h=\{v\in C(\Omega):v|_\kappa\in P_1(\kappa),\forall\kappa\in\Gamma\},$$

where $P_1(\kappa)$ denotes the space of polynomials of degree 1 over κ. Then the finite element discretization of (2.1)-(2.4) is: find $\mathbf{u}_h\in(S_h)^2$ such that

$$\begin{cases}\left(M\frac{\partial\mathbf{u}_h}{\partial t},\mathbf{v}_h\right)+K(\nabla\mathbf{u}_h,\nabla\mathbf{v}_h)=(\mathbf{f},\mathbf{v}_h), & \forall\mathbf{v}_h\in(S_h)^2,\\ (\mathbf{u}_h(\mathbf{x},0),\mathbf{v}_h)=(\mathbf{u}_h^0,\mathbf{v}_h), & \forall\mathbf{v}_h\in(S_h)^2,\end{cases}\tag{2.8}$$

where

$$\mathbf{u}_h^0(\mathbf{x}):=\left(a_h^0(x,y),h_h^0(x,y)\right)^T\in(S_h)^2$$

is the finite element approximation to $\mathbf{u}^0(\mathbf{x}):=\left(a^0(x,y),h^0(x,y)\right)^T$.

A two stage second order Runge-Kutta scheme is employed for the time discretization. For the nonlinear reaction term (2.7), an implicit-explicit time integration method is used, which is presented in [27–29]. Let $0=t_0<t_1<\cdots<t_N=T$ be a subdivision of $[0,T]$ with corresponding time steps $\Delta t=t_{n+1}-t_n$. If we define $\mathbf{u}_h^n$ to be the finite element approximation to $\mathbf{u}$ at time t_n, the full discretization of (2.8) is given as follows:

Stage 1:

$$\left(M\frac{\mathbf{u}_h^{(1)}-\mathbf{u}_h^n}{\Delta t},\mathbf{v}_h\right)+K(\nabla\mathbf{u}_h^{(1)},\nabla\mathbf{v}_h)=(\mathbf{f}(\mathbf{u}_h^n,\mathbf{x}),\mathbf{v}_h),\quad\forall\mathbf{v}_h\in(S_h)^2.$$
$$(\mathbf{u}_h(\mathbf{x},0),\mathbf{v}_h)=(\mathbf{u}_h^0,\mathbf{v}_h),\quad\forall\mathbf{v}_h\in(S_h)^2.$$

Stage 2:

$$\left(M\frac{\mathbf{u}_h^{n+1}-\mathbf{u}_h^n}{\Delta t},\mathbf{v}_h\right)+K(\nabla\mathbf{u}_h^{n+1},\nabla\mathbf{v}_h)=(\frac{\mathbf{f}(\mathbf{u}_h^{(1)},\mathbf{x})+\mathbf{f}(\mathbf{u}_h^n,\mathbf{x})}{2},\mathbf{v}_h),\quad\forall\mathbf{v}_h\in(S_h)^2.$$
$$(\mathbf{u}_h(\mathbf{x},0),\mathbf{v}_h)=(\mathbf{u}_h^0,\mathbf{v}_h),\quad\forall\mathbf{v}_h\in(S_h)^2.$$

2.2 Moving mesh strategy

Assume that we have obtained a finite element solution (a_h^n,h_h^n) at $t=t_n$ on the mesh Γ^n using the methods describe in section 2.1. The outline of our moving mesh algorithm is as follows :

- Step 1 : Solve the Euler-Lagrange equation

$$\begin{aligned}&\frac{\partial}{\partial x_i}(G^{ij}\frac{\partial\xi^k}{\partial x_j})=0,\quad\mathbf{x}\in\Omega,\\ &\vec{\xi}|_{\partial\Omega}=\vec{\xi}_b,\end{aligned}\tag{2.9}$$

  to obtain a logical mesh $\vec{\xi}^*$, where $G=(G^{ij})=M^{-1}$. M is called monitor function.

- Step 2 : Judge if L_2-norm of $\vec{\xi}^*-\vec{\xi}^0$ is small enough, where $\vec{\xi}^0$ is the fixed initial logical mesh. If yes, the iteration is over. Otherwise, do the following procedure.
- Step 3 : Using the difference $\vec{\xi}^*-\vec{\xi}^0$ to compute the mesh-moving vector $\delta\vec{x}$ in the physical domain. Then select a suitable ration parameter $\lambda\in[0,1]$, and move the old mesh $\Gamma^{n,s}$ in the physical domain to a new one $\Gamma^{n,s+1}$ by using

$$\vec{x}_0^{n+1}=\vec{x}_0^n+\lambda\delta\vec{x}_0.$$

- Step 4 : Update the numerical approximation at the new mesh $\Gamma^{n,s+1}$.

The above steps are repeated until the L_2 norm of $\vec{\xi}^*-\vec{\xi}^0$ is small enough. Then a new mesh Γ^{n+1} at $t=t_{n+1}$ is obtained, and the given PDEs are solved on the new mesh. The detailed moving mesh procedure can be found in [12, 13].

In this work, the monitor function is chosen as

$$M=\sqrt{1+\beta\frac{|a|^2}{\max|a|^2}+\gamma\frac{|\nabla a|^2}{\max|\nabla a|^2}}, \tag{2.10}$$

where β and γ are some non-negative constants, see, e.g., [30].

3 Spike dynamics when $\tau=0$

3.1 One spike dynamics

From [10], we have the following lemma:

Lemma 3.1. *Let $\mu=1, V(x)=0$, and Ω be the unit circle. Suppose that the spike is initially centered at $x_0(0)\in\Omega$. Then, when $\epsilon\ll 1$ and $D\gg 1$, the distance from the spike to the origin at later times is given by*

$$\|x_0(t)\|\sim(1-[1-\beta e^{-2\epsilon^2 kt}]^{\frac{1}{2}})^{\frac{1}{2}}, \tag{3.1}$$

where

$$\beta=1-(1-|x_0(0)|^2)^2, \tag{3.2}$$

$$k=\frac{2q}{D(p-1)}. \tag{3.3}$$

For $(p,q,r,s)=(2,1,2,0)$, $V(x)=0, \mu(x)=1$, we solve the system (2.1)-(2.4) in a unit circular domain with a triangular mesh. The initial condition is chosen as

$$\begin{cases} a(x,0)=\operatorname{sech}^8[\epsilon^{-1}|x-x_1|], \\ h(x,0)=100, \end{cases} \tag{3.4}$$

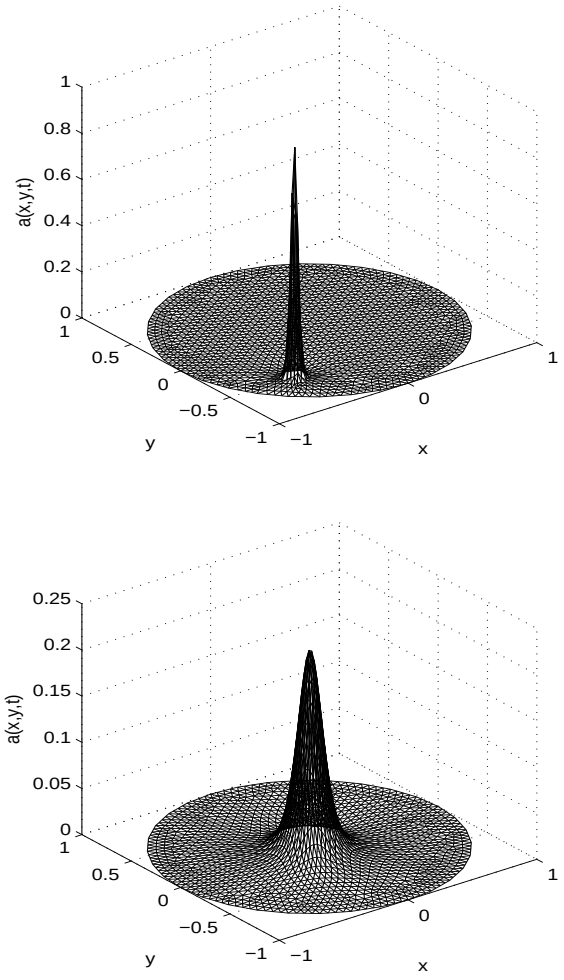

Figure 1: One spike dynamics: the activator $a(x,y,t)$ at $t=0$ (top) and $t=5000$ (bottom).

where $x_1=(-0.5,-0.5)$. There will be a single spike in the activator concentration centered at (-0.5,-0.5) at the initial time. Then the asymptotic distance of the spike to the origin is given in (3.1).

In Figs. 1 and 2, we give the profile of $a(x,y,t)$ at $t=0$ and $t=5000$, and also the corresponding mesh figures. From the mesh figures, we can see that there are more mesh points clustered inside the spatial extension of the spikes. In Fig. 3(a), when $D=10$ and $\epsilon=0.06$, we show the close agreement between the full numerical result using our moving FEM with time step $\Delta t=0.1$ for the distance of the spike to the origin and the asymptotic result obtain from (3.1). In Fig. 3(b), the comparison between the full numerical result by FEM on uniform mesh and the asymptotic result is given. The distance figure obtained

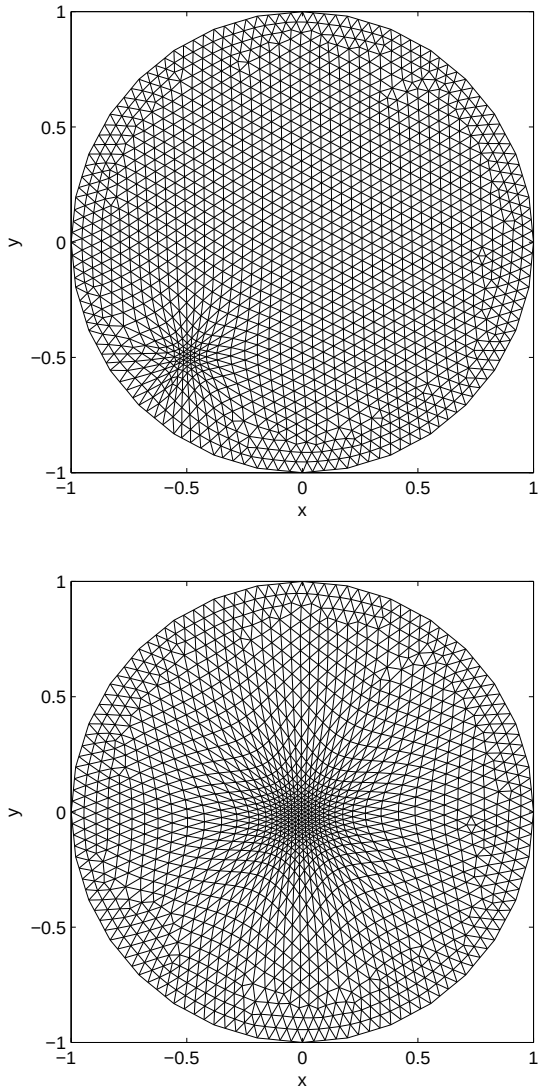

Figure 2: One spike dynamics: the adaptive mesh at $t=0$ (top) and $t=5000$ (bottom).

with $\Delta t=0.05$ is given in Fig. 3(c). We compare the motion of the center of the spike in Table 1. We also compare the numerical results using our method with different time step $\Delta t=0.1$ and $\Delta t=0.05$ in Table 2. From the figures and tables, it can be seen that we get a good numerical result with less elements using the moving FEM. In the numerical computations, we take 1598 nodes and 3066 elements for the moving FEM, 9290 nodes and 18258 elements for the FEM on a uniform mesh.

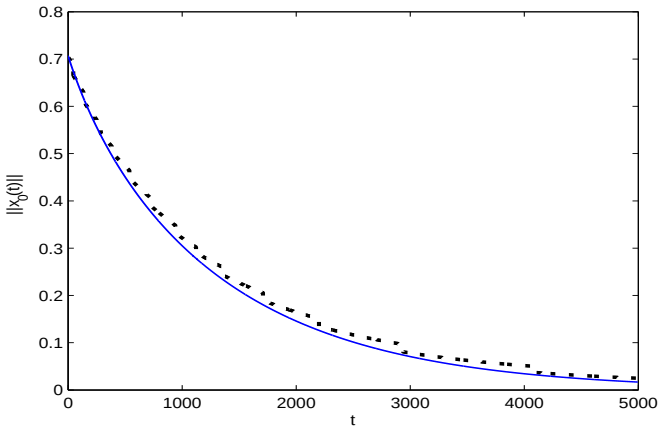

(a)

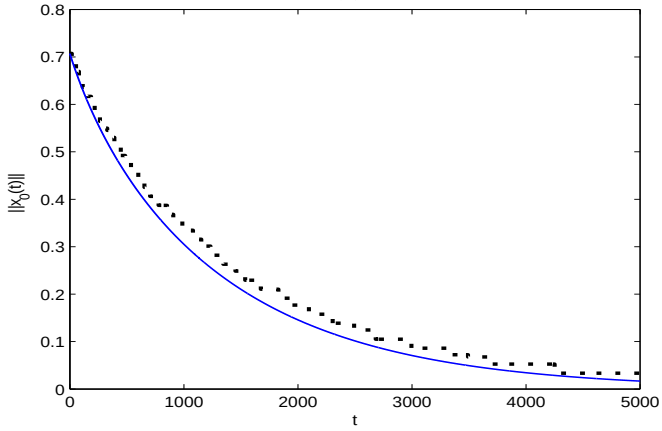

(b)

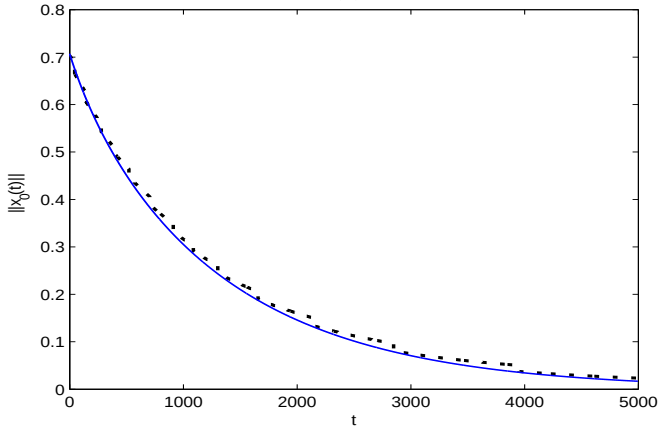

(c)

Figure 3: The distance from the center of the spike to the origin when $D=10$ and $\epsilon=0.06$ in one spike dynamics. The solid curves are the asymptotic results from (3.1), and the dashed curves correspond to (a): $\Delta t=0.1$, moving mesh with 3066 elements; (b): $\Delta t=0.1$, fixed mesh with 18258 elements; (c): $\Delta t=0.05$, moving mesh with 3066 elements.

Table 1: The asymptotic results of $\|x_0(t)\|$ obtained from (3.1) and the numerical results of $\|x_0(t)\|$ obtained using the finite element method on a moving grid (MFEM) with 3066 elements and on a fixed mesh (FEM) with 18258 elements when $\Delta t=0.1$.

t	$\|x_0(t)\|$(ASY)	$\|x_0(t)\|$(MFEM)		$\|x_0(t)\|$(FEM)
		RK2	Euler	
t=100	0.6387	0.6432	0.6452	0.6551
t=200	0.5817	0.5881	0.5914	0.6025
t=400	0.4894	0.5108	0.5160	0.5114
t=800	0.3557	0.3744	0.3820	0.3870
t=1200	0.2627	0.2799	0.2880	0.3012
t=1600	0.1954	0.2162	0.2241	0.2295
t=2000	0.1459	0.1650	0.1724	0.1769

Table 2: Comparison of the numerical results of $\|x_0(t)\|$ obtained from the moving mesh solution using Runge-Kutta method with different time step.

t	$\|x_0(t)\|(\Delta t=0.1)$	$\|x_0(t)\|(\Delta t=0.05)$
t=100	0.6432	0.6417
t=200	0.5881	0.5858
t=400	0.5108	0.4954
t=800	0.3744	0.3695
t=1200	0.2799	0.2747
t=1600	0.2162	0.2113
t=2000	0.1650	0.1603

3.2 Two spikes dynamics

The stability of multispike solutions to the GM model in a multidimensional domain is a difficult problem. Only a few analysis results on this problem. In [24], it was proved that when $V(x)=0,\mu=1$, for $\epsilon\to 0$, an K-spike equilibrium solution is stable on $\mathcal{O}(1)$ time scale if and only if

$$D<D_K=\frac{|\Omega|}{2\pi K}\log\frac{1}{\epsilon}. \tag{3.5}$$

In [10], the authors has done the numerical simulation of this problem on an extremely fine uniform mesh. We also do the simulation based on the moving finite element method. The profiles of $a(x,y,t)$ at $t=0$ and $t=5000$ are shown in Fig. 4 with $K=2$, $\epsilon=0.03$ and $D=0.5$. It is found that the two-spike equilibrium solution is stable when $K=2$, $\epsilon=0.03$ and $D=0.5$. From (3.5), we get when $D<D_K=0.88$, the two-spike equilibrium solution is stable. So the numerical results agree well with the analysis results (3.5). However, in [10], what the authors got is $D_K=0.28$. So they believed that the formula (3.5) from [24] should be modified. But in fact, the authors of [10] mis-cited the formula.

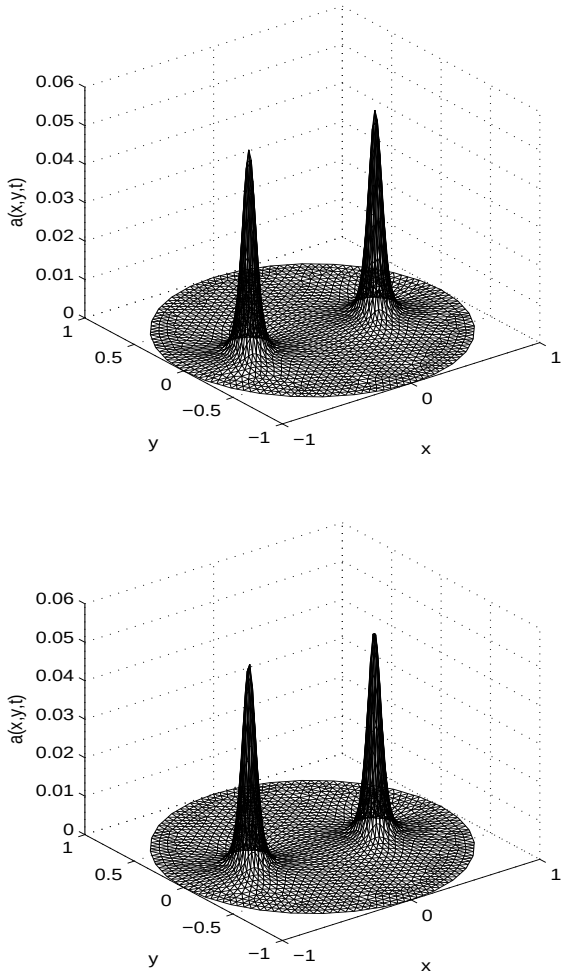

Figure 4: Two spike dynamics: the activator $a(x,y,t)$ at $t=100$ (top) and $t=5000$ (bottom) when $D=0.5$ and $\epsilon=0.03$.

What they used is

$$D<D_K=\frac{1}{2\pi K}\log\frac{1}{\epsilon}. \tag{3.6}$$

They dropped the area of the domain in the formula, and as a result the value of D_K used in [10] is much smaller than the real one.

We also do another simulation with the same parameter values for $D,\epsilon,V(x)$ and μ as in one spike dynamics in Section 3.1. Then from (3.5) we know $D>D_K$ means the K-peaked solution is unstable. In Fig. 5, we give the figures for $a(x,y,t)$ at different time and the corresponding mesh figures. From the simulation, we have observed that one of the spikes is annihilated quickly, while the remaining spike drifts very slowly toward

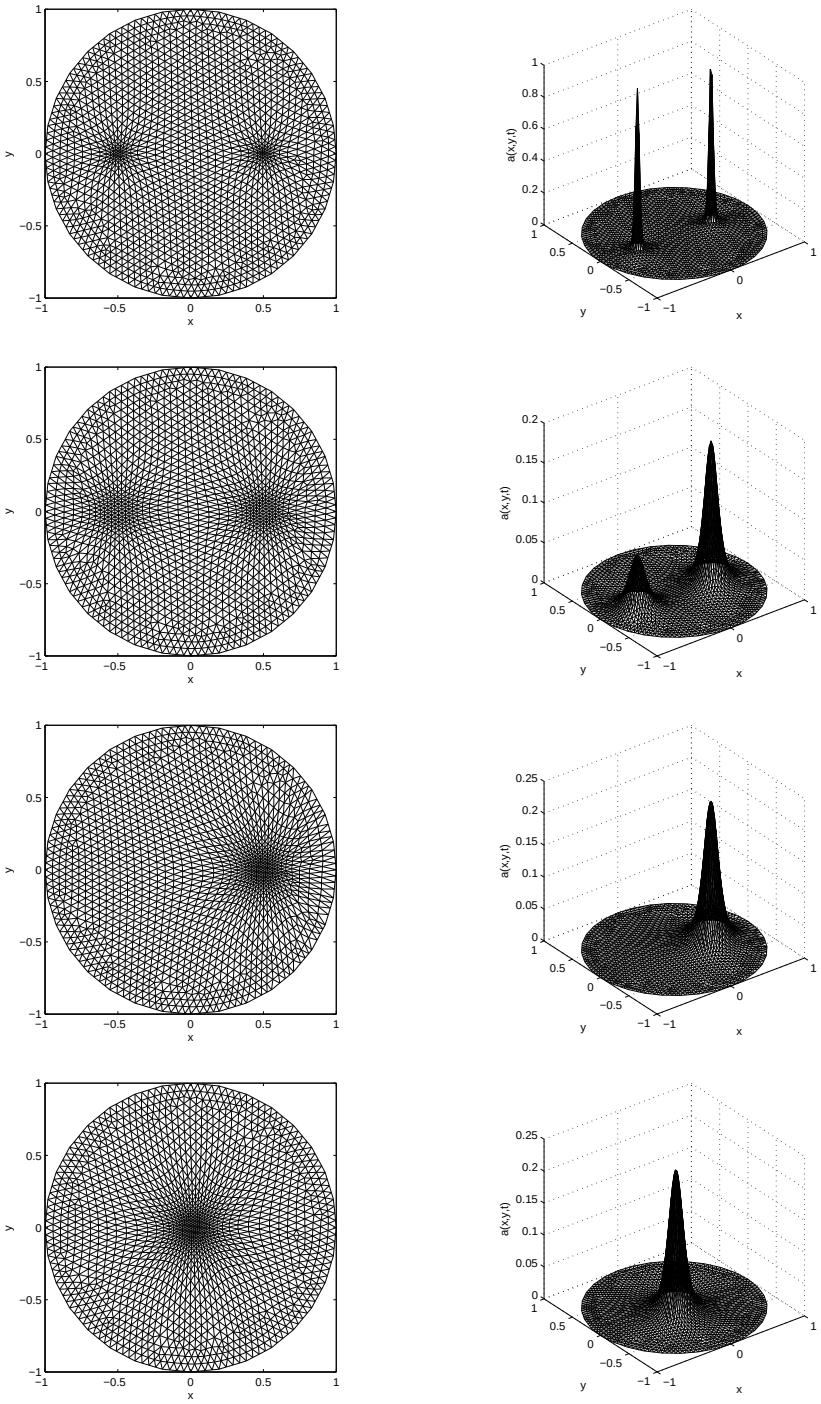

Figure 5: The profiles of $a(x,y,t)$ (right) at different times and the corresponding meshes (left) when $D=10$ and $\epsilon=0.06$.

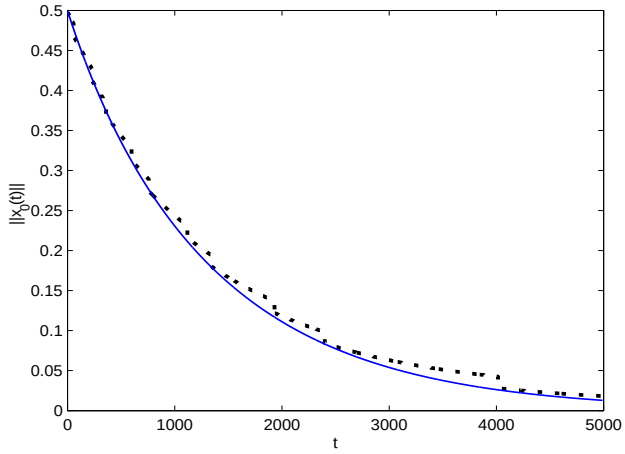

Figure 6: The distance from the center of the remaining spike to the origin for numerical example when $D=10$ and $\epsilon=0.06$ in two spike dynamics. The dotted curve is the result using moving FEM with the mesh of 3066 elements, and the solid curve is the asymptotic result from (3.1) .

the center of the circle. Furthermore, the parameters satisfy the conditions in Lemma 3.1, so we expect that the distance from the center of the remaining spike to the origin is also given by (3.1). The Fig. 6 proves it.

In our experiment of this subsection, the initial conditions are

$$\begin{cases} a(x,0)=\sum_{i=1}^{m}\operatorname{sech}^8[\epsilon^{-1}|x-x_i|], \\ h(x,0)=100, \end{cases} \tag{3.7}$$

where $m=2, x_1=(-0.5,0), x_2=(0.5,0)$. This initial condition will give two spikes of a localized at two points x_1, x_2.

4 Spike dynamics when $\tau>0$

4.1 Oscillations

It is observed in [14] that in one space dimension when the spike is placed at the center of the domain, it will not move. It is also found that when D is specified, there is a critical value τ_0 such that when $\tau<\tau_0$, the spike will oscillate damply to a stable state; and when $\tau>\tau_0$, the spike will have a persistent oscillation.

Here we consider a two-dimensional problem. We expect that the above properties in one space dimension still exist. Take a square domain, and put an initial concentration of a and h in the center of the square. Let a be more localized than h. In our experiment of this subsection, the initial conditions are of the form

$$a=\frac{3\mathcal{H}}{2}\operatorname{sech}^2\left(\frac{\sqrt{x^2+y^2}}{2\epsilon^2}\right)(1+\delta v), \quad h=\frac{\mathcal{H}\cosh[l(1-\sqrt{x^2+y^2})]}{\cosh l}, \tag{4.1}$$

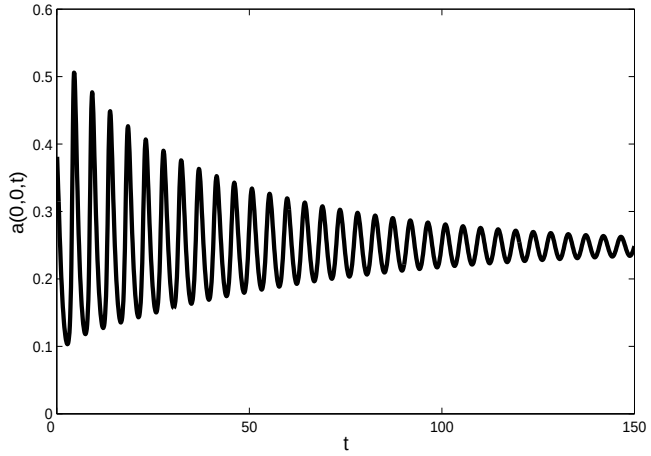

(a) $\tau=0.75$

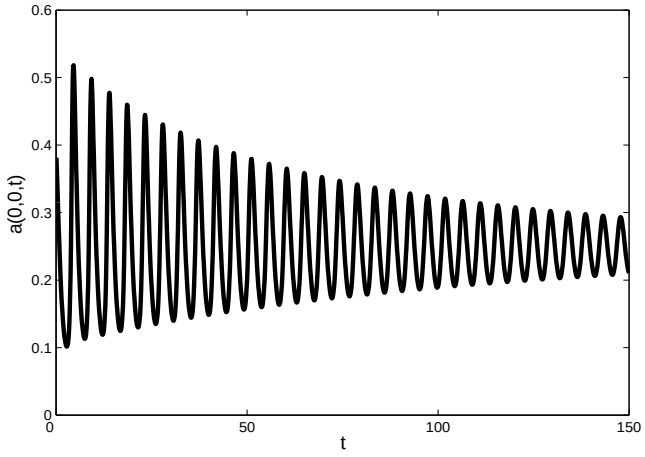

(b) $\tau=0.76$

Figure 7: The model (2.1)-(2.4) with initial data (4.1) for the oscillation simulation problem 4.1: Plots of $a(0,0,t)$ versus t when $D=10$, $\epsilon=0.04$ and $\tau<\tau_0$.

where

$$v=\sum_{k=1}^{20}\cos(\frac{k\pi y}{2}),\quad \mathcal{H}=\frac{1}{3l},\quad l=1,\quad \text{and } \delta=0.001.$$

These initial conditions will put Gaussian profiles with a more localized than h at the center of the square.

Through the computations in this subsection, we let $D=10$ and $\epsilon=0.04$. It is observed that the critical τ_0 is about 0.77. In Fig. 7, we plot $a(0,0,t)$ when $\tau<0.77$. It can be seen that the spike at the origin oscillates and tends to a stable state gradually. And when τ becomes smaller, the time to the stable state becomes shorter. In Fig. 8, we plot $a(0,0,t)$ when $\tau\geq 0.77$. It can be seen that the spike at the origin oscillates persistently. Moreover, when τ becomes larger, the magnitude of the oscillation becomes larger.

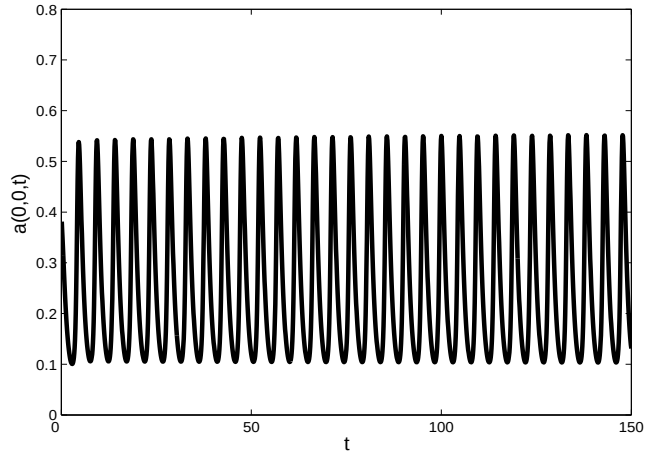

(a) $\tau = 0.77$

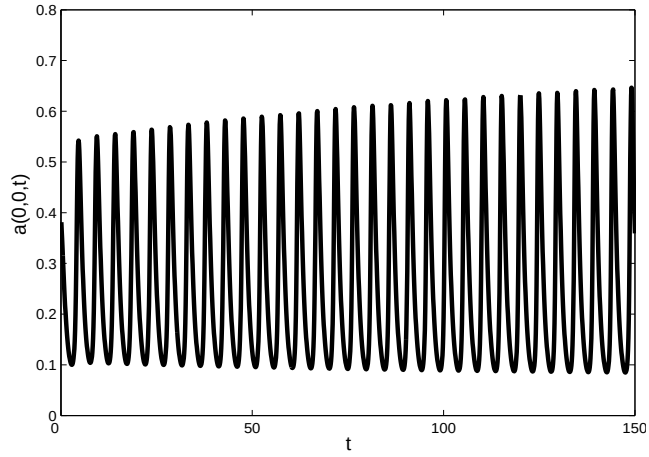

(b) $\tau = 0.773$

Figure 8: The model (2.1)-(2.4) with initial data (4.1) for the oscillation simulation problem 4.1: Plots of $a(0,0,t)$ versus t when $D = 10$, $\epsilon = 0.04$ and $\tau > \tau_0$.

4.2 Pulse splitting

In 1D GM model, if τ is specified, when the value of D is at the level of $\mathcal{O}(\epsilon^2)$, there will be some pulse splitting phenomenon, see for example, [14]. Now we try to simulate these phenomenon in the 2D case.

Take $\epsilon = 0.04$, $D = D_0\epsilon^2$ and $\tau = 0.1$, and put an initial concentration of a and h at the center of the square taking the initial conditions (4.1). From the numerical simulations, we found that the spike at the center will be splitting and the domain will be filled with spikes as t increases when D_0 is less than 10.0. This is the two-dimensional equivalence of a phenomena observed in [14]. Furthermore, when we choose different D_0 which is less than 10.0, it is found that different patterns will be formed. In Figs. 9-10, we take

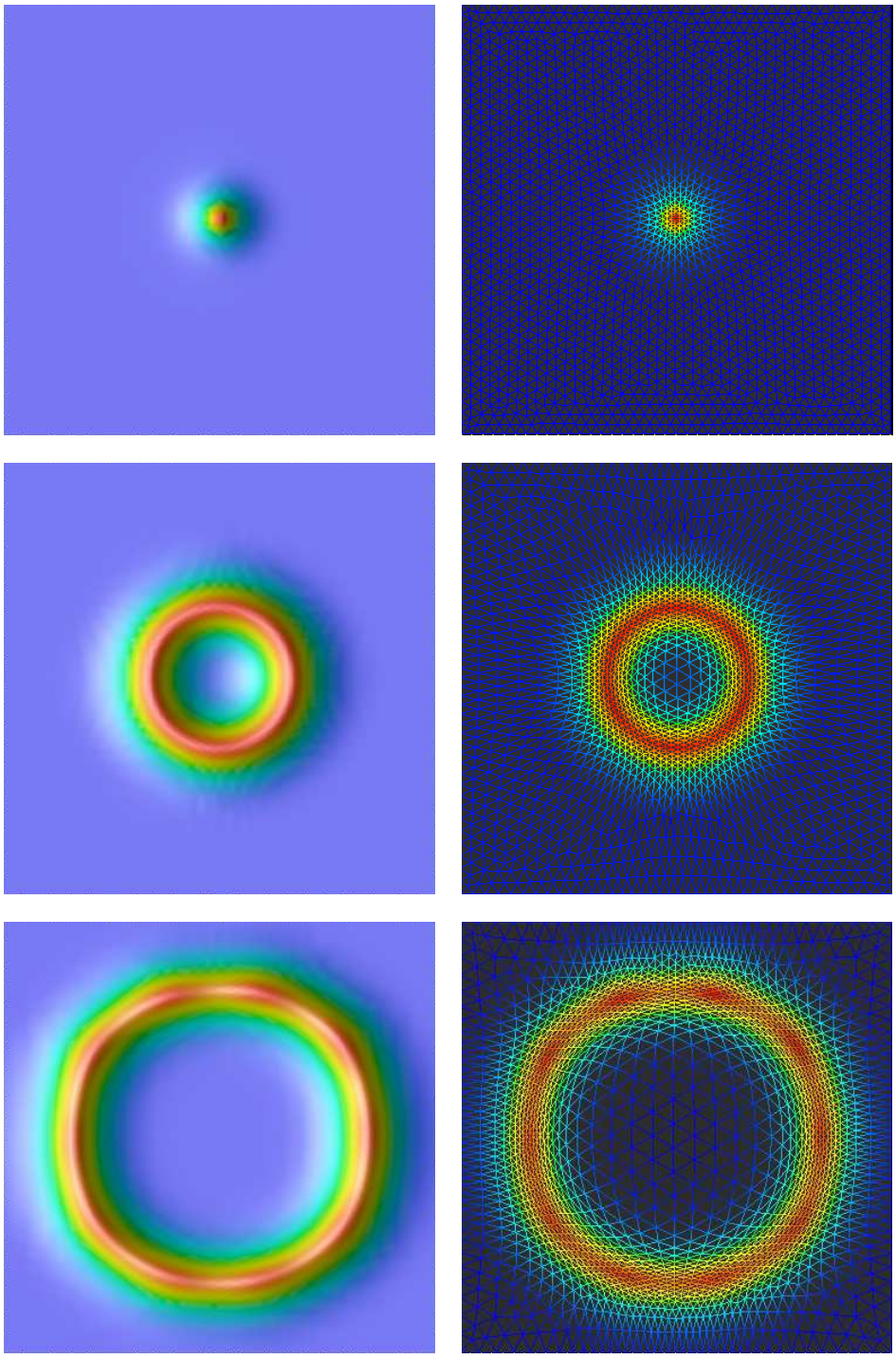

Figure 9: Graphs of patterns at $t=0$, $t=50$, $t=200$ and the corresponding meshes when $D_0=8.0$, $\epsilon=0.04$ and $\tau=0.1$ for pulse spitting simulation.

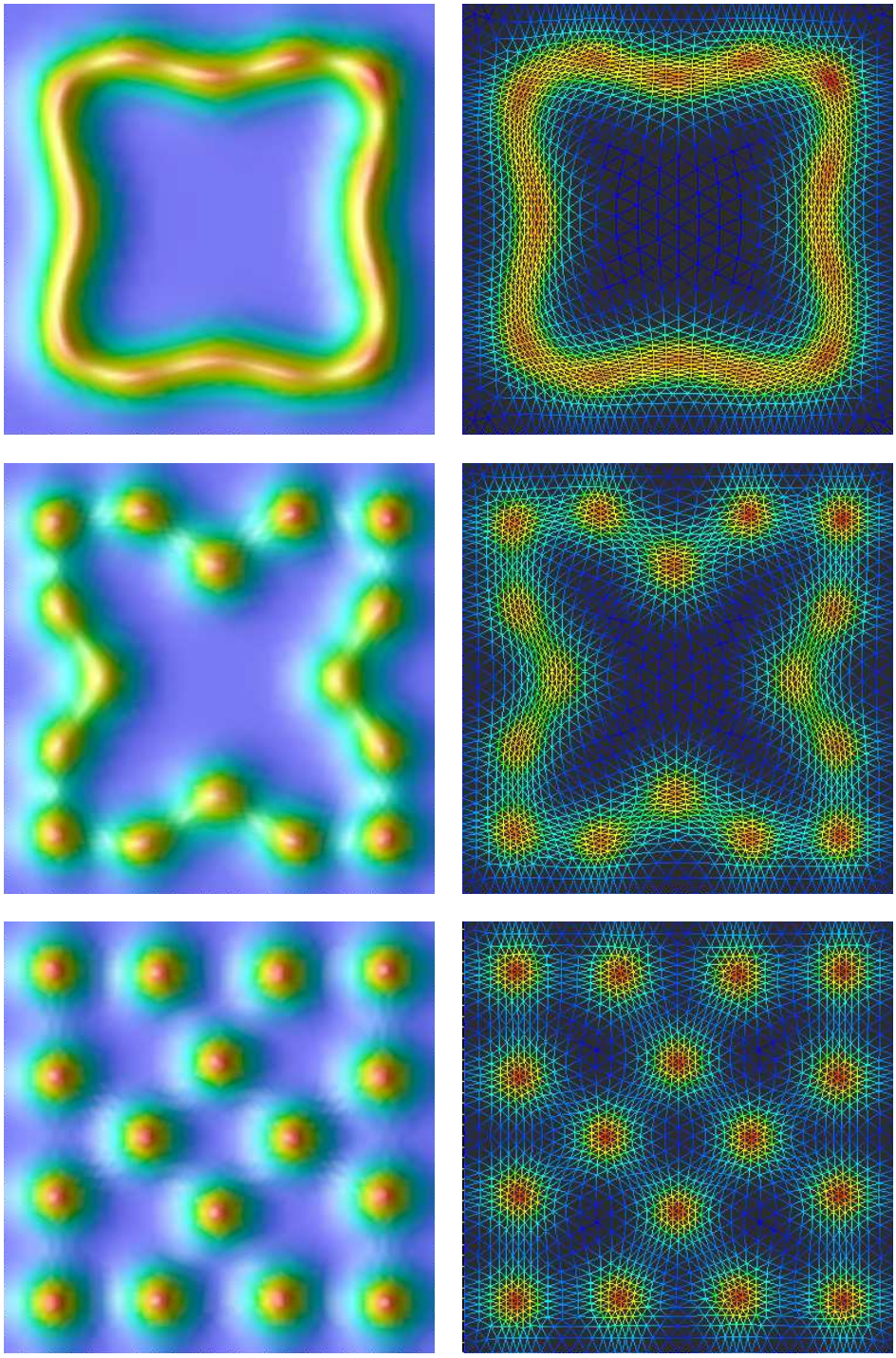

Figure 10: Same as Fig. 9, except at $t=300$, $t=350$, $t=500$.

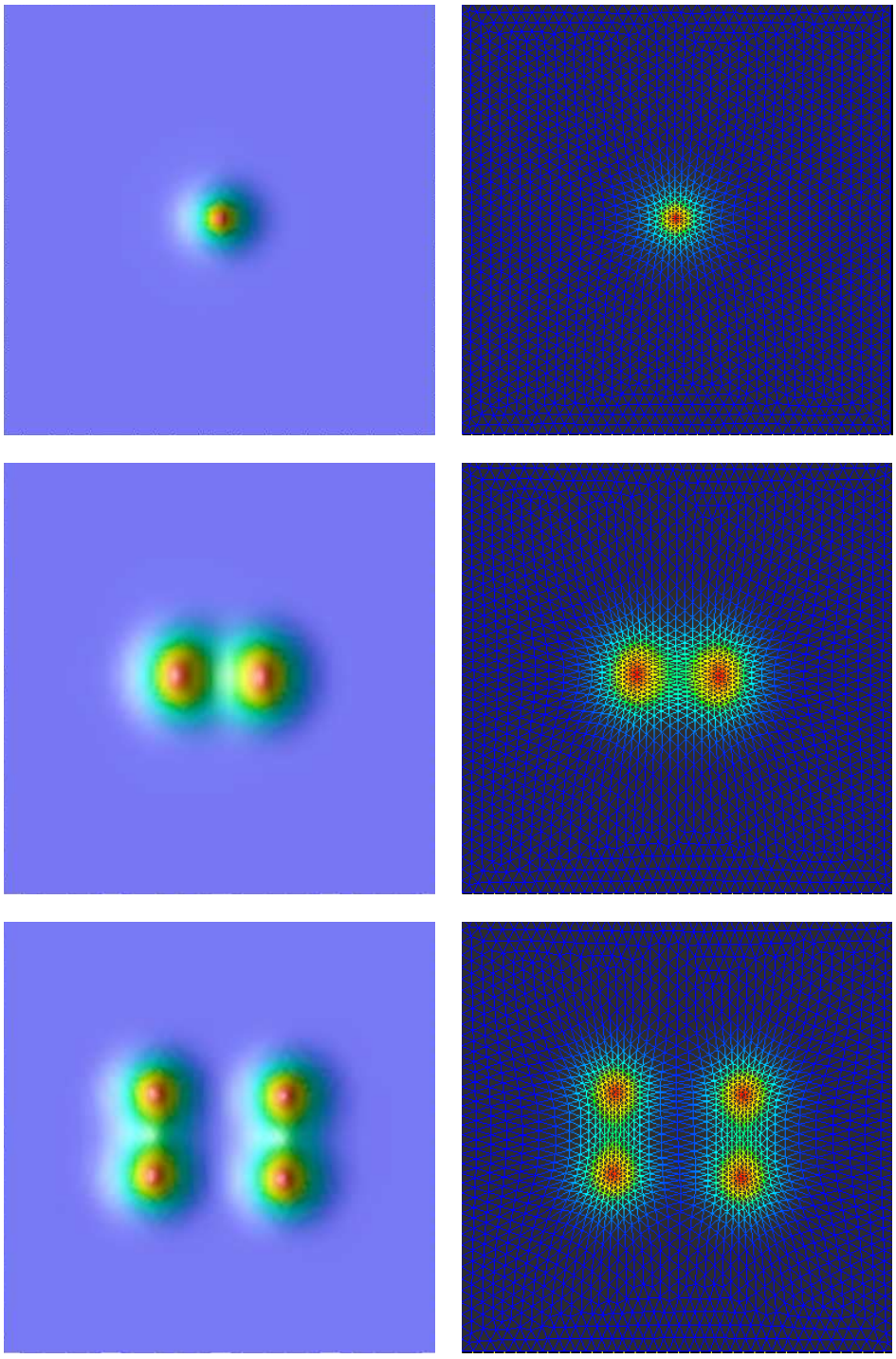

Figure 11: Graphs of patterns at $t=0$, $t=50$, $t=100$ and the corresponding meshes when $D_0=9.5$, $\epsilon=0.04$ and $\tau=0.1$ for pulse spitting simulation.

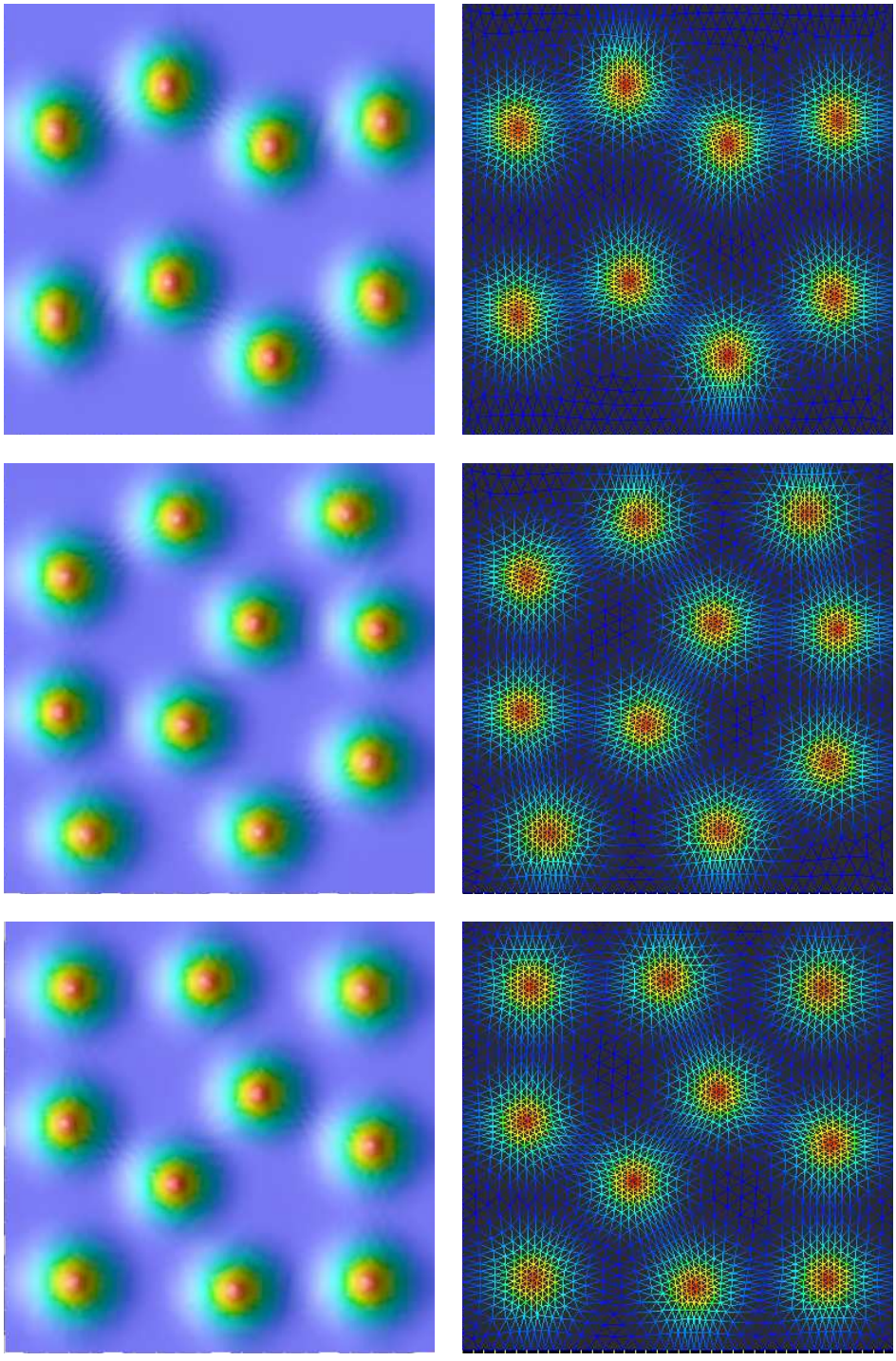

Figure 12: Same as Fig. 11, except at $t=500$, $t=800$, $t=2000$.

$D_0 = 8.0$, and then the spike splits to a steady state at $t = 500$. In Fig. 9, we can find that the spike begins to split to a ring when $t = 50$. The ring becomes bigger and bigger. Then the ring becomes almost square and subsequently the four edges of the square become sunken in the middle, and then the whole annulation splits to spikes which fill the domain with some symmetry, see Fig. 10. When $D_0 = 9.5$, we have obtained different pattern formations as observed in Figs. 11 and 12. It is observed that the single spike splits to 2 and 4 spikes in Fig. 11. There are 8 spikes at $t = 300$ and $t = 500$, and 9 spikes at $t = 600$. From $t = 800$ to 2000, the number of spikes stays with a constant, although their positions change slowly.

We close this section by one observation. In the numerical simulations, when D is small, the value of $a(x,y,t)$ becomes very small accordingly. Therefore it is necessary to make some scaling changes. For example, if we define

$$u = \epsilon^{-1} a, \quad v = \epsilon^{-1} h, \tag{4.2}$$

then (2.1)-(2.4) will become

$$u_t = \epsilon^2 \Delta u - u + \frac{u^2}{v}, \quad x \in \Omega, \quad t > 0, \tag{4.3}$$

$$\tau v_t = D\Delta v - v + \epsilon^{-1} u^2, \quad x \in \Omega, \quad t > 0, \tag{4.4}$$

$$\partial_n u = \partial_n v = 0, \quad x \in \partial\Omega, \tag{4.5}$$

$$u(x,y,0) = u^0(x,y), \quad v(x,y,0) = v^0(x,y). \tag{4.6}$$

The scaling technique can make the numerical computation more stable. In some literature, see e.g., [22–24], the scaling technique was used to study the GM model for simplicity.

5 Conclusions

In this work, we applied a moving mesh finite element method to 2D GM models modeling spike dynamics in pattern formation. We were successful in distributing mesh points into the spatial extension of the spikes, even as the spikes have various dynamical behaviors. The role of two parameters in the GM model (1.1)-(1.4), ϵ (activator diffusivity) and τ (inhibitor time constant), is investigated. The numerical strategy is found very efficient in resolving the spike dynamics with very small ϵ. When $\tau = 0$, when $D = 0.5$ and $\epsilon = 0.03$, it was found that the two-spike system is stable. For $D = 10$ and $\epsilon = 0.06$, the two spikes become unstable. When $\tau > 0$, we have taken a glimpse on some two-dimensional equivalence of phenomenon observed in the one-dimensional domain. Different kinds of instability are captured in a two-dimensional domain. In particular, when $D = D_0\epsilon^2$, it was observed that different behaviors including rings, ring-splitting and pulse-splitting can occur.

References

[1] H. Meinhardt, Models of Biological Pattern Formation, Academic Press, London, 1982.
[2] H. Meinhardt, The Algorithmic Beauty of Sea Shells, Springer-Verlag, Berlin, 1995.
[3] A. Turing, The chemical basis of morphogenesis, Philos. T. Roy. Soc. B, 237 (1952), 32-72.
[4] D. Holloway, Reaction-diffusion theory of localized structures with applications to vertebrate organogenesis, Ph.D. Thesis, Dept. of Chemistry, Univ. of British Columbia, Vancouver, Canada, 1995.
[5] A. Gierer and H. Meinhardt, A theory of biological pattern formation, Kybernetik, 12 (1972), 30-39.
[6] P. Gray and S. K. Scott, Sustained oscillations and other exotic patterns of behaviour in isothermal reactions, J. Phys. Chem., 59 (1985), 22-32.
[7] J. Schnakenberg, Simple chemical reaction systems with limite cycle behavior, J. Theor. Biol., 81 (1979), 389-400.
[8] M. I. Granero, A. Porati and D. Zanacca, A bifurcation analysis of pattern formation in a diffusion governed morphogenetic field, J. Math. Biol., 4 (1977), 21-27.
[9] A. Hunding, Morphogen prepatterns during mitosis and cytokinesis in flattened cells: Three-dimensional Turing structures of reaction-diffusion systems in cylindrical coordinates, J. Theor. Biol., 114 (1985), 571-588.
[10] M. J. Ward, D. Mcinerney and P. Houston, The dynamics and pinning of a spike for a reaction-diffusion system, SIAM J. Appl. Math., 62 (2002), 1297-1328.
[11] M. J. Ward and J. Wei, Hopf bifurcation and oscillatory instabilities of spike solutions for the one-dimensional Gierer-Meinhardt model, J. Nonlinear Sci., 13 (2003), 209-264.
[12] R. Li, T. Tang and P. W. Zhang, Moving mesh methods in multiple dimensions based on harmonic maps, J. Comput. Phys., 170 (2001), 562-588.
[13] R. Li, T. Tang and P. Zhang, A moving mesh finite element algorithm for singular problems in two and three space dimensions, J. Comput. Phys., 177 (2002), 365-393.
[14] W. Sun, T. Tang, M. J. Ward and J. Wei, Numerical challenges for resolving spike dynamics for two reaction-diffusion systems, Studies in Applied Math., 111 (2003), 41-84.
[15] T. Kolokolnikov and M. J. Ward, Bifurcation of spike equilibria in the near-shadow Gierer-Meinhardt model, Dis. Cont. Dyn. Sys. B, 4 (2004), 1033-1064.
[16] G. Beckett, J. A. Mackenzie and M. L. Robertson, An r-adaptive finite element method for the solution of the two-dimensional phase-field equations, Commun. Comput. Phys., 1 (2006), 805-826.
[17] H. D. Ceniceros and T. Y. Hou, An efficient dynamically adaptive mesh for potentially singular solutions, J. Comput. Phys., 172 (2001), 609-639.
[18] Y. Di and P. Zhang, Moving mesh kinetic simulation for sheared rodlike polymers with high potential intensities, Commun. Comput. Phys., 1 (2006), 859-873.
[19] W. M. Cao and W. Z. Huang and R. D. Russell, An *r*-adaptive finite element method based upon moving mesh PDEs, J. Comput. Phys., 149 (1999), 221-244.
[20] K. Lipnikov and M. Shashkov, The error-minimization-based strategy for moving mesh methods, Commun. Comput. Phys., 1 (2006), 53-80.
[21] P. A. Zegeling, On resistive MHD models with adaptive moving meshes, J. Sci. Comput, 24 (2005), 263-284.
[22] T. Kolokolnikov, W. Sun, M. J. Ward and J. Wei, The stability of a stripe for the Gierer-Meinhardt model and the effect of saturation, SIAM J. Appl. Dyn. Syst., accepted.
[23] J. Wei and M. Winter, On the two-dimensional Gierer-Meinhardt system with strong coup-

ing, SIAM J. Math. Anal., 30 (1999), 1241-1263.
[24] J. Wei and M. Winter, Spikes for the two-dimensional Gierer-Meinhardt system: the weak coupling case, J. Nonlinear Sci., 11 (2001), 415-458.
[25] D. Iron and M. J. Ward, The dynamics of multispike solutions to the one-dimensional Gierer-Meinhardt model, SIAM J. Appl. Math., 62 (2002), 1924-1951.
[26] D. Iron, M. J. Ward and J. Wei, The stability of spike solutions to the one-dimensional Gierer-Meinhardt model, Physica D, 150 (2001), 25-62.
[27] G. Akrivis, M. Crouzeix and C. Makridakis, Implicit-explicit multistep finite element methods for nonlinear parabolic problems, Math. Comput., 67 (1998), 457-477.
[28] U. M. Ascher, S. J. Ruuth and Brian T. R. Wetton, Implicit-explicit methods for time-dependent partial differential equations, SIAM J. Numer. Anal., 32 (1995), 797-823.
[29] S. J. Ruuth, Implicit-explicit methods for reaction-diffusion problems in pattern formation, J. Math. Biol., 34 (1995), 148-176.
[30] H.-Z. Tang, A moving mesh method for the Euler flow calculations using a directional monitor function, Commun. Comput. Phys., 1 (2006), 656-676.
[31] L. Harrison and D. Holloway, Order and localization in reaction-diffusion pattern, Physica A, 222 (1995), 210-233.
[32] X. Chen and M. Kowalczyk, Dynamics of an interior spike in the Gierer-Meinhardt system, SIAM J. Math. Anal., 33 (2001), 172-193.